Lower Hybrid Current Drive at High Density in Alcator C-Mod

G.M. Wallace 1), A.E. Hubbard 1), P.T. Bonoli 1), R.W. Harvey 2), J.W. Hughes 1), B.L. LaBombard 1), O. Meneghini 1), R.R. Parker 1), A.E. Schmidt 1), S. Shiraiwa 1), A.P. Smirnov 2), D.G. Whyte 1), J.R. Wilson 3), J.C. Wright 1), S.J. Wukitch 1), and the Alcator C-Mod Team

1) MIT Plasma Science and Fusion Center, Cambridge, MA 02139, USA 2) CompX, Del Mar, CA 92014, USA 3) Princeton Plasma Physics Laboratory, Princeton, NJ 08543, US

E-mail contact of main author: wallaceg@mit.edu

Abstract. Experimental observations of lower hybrid current drive (LHCD) at high density on the Alcator C-Mod tokamak are presented in this paper. Bremsstrahlung emission from relativistic fast electrons in the core plasma drops suddenly above line averaged densities of 10^{20} m^{-3} ($\omega/\omega_{LH} \sim 3$) in single null discharges with large (> 10 mm) plasma–inner wall gaps, well below the density limit previously observed on limited tokamaks ($\omega/\omega_{LH} \sim 2$). Modeling and experimental evidence suggest that the absence of LHCD driven fast electrons at high density may be due to parasitic collisional absorption in the scrape off layer. Experiments show that the population of fast electrons produced by LHCD at high density ($\bar{n}_e >$ m^{-3}) can be increased significantly by operating with a plasma–inner wall gap of less than ~ 5 mm with the strongest non-thermal emission in inner-wall limited plasmas. A change in plasma topology from single to double null produces a modest increase in non-thermal emission at high density. Increasing the electron temperature in the periphery of the plasma ($0.8 > r/a > 1.0$) also results in a modest increase in non-thermal electron emission above the density limit.

1. Introduction

Tokamak experiments require a toroidal current to provide plasma confinement. This toroidal current is conventionally driven by transformer action, although relying solely on inductive current drive limits the maximum duration of the pulse. Lower hybrid (LH) waves can be used on tokamak experiments as a means of generating non-inductive current [1]. Lower hybrid current drive (LHCD) is a particularly attractive method of driving non-inductive current due to its high current drive efficiency, $\eta = n_e I_P R_0 / P_{LH} \sim 0.1 \times 10^{20}$ m^{-2}MW^{-1}MA, and ability to drive current off axis.

The LHCD system [2] on the Alcator C-Mod tokamak [3] is designed to investigate current profile control under plasma conditions relevant to future devices such as ITER and DEMO. This paper addresses the behavior of Lower Hybrid (LH) waves in a compact, high field, high density, diverted tokamak. The C-Mod LHCD system has demonstrated efficient current drive at line averaged densities below 1×10^{20} m^{-3} [4], however the current drive efficiency in single null discharges is substantially reduced above the "density limit" of $\bar{n}_e \sim 1 \times 10^{20}$ m^{-3} [5, 6, 7]. This critical density associated with reduced current drive in the core plasma on C-Mod is unusual in that it occurs at a density significantly lower ($\omega/\omega_{LH} \sim 3$) than what would have been expected based on scaling laws from prior LHCD experiments ($\omega/\omega_{LH} \sim 2$) [8, 9]. Here, $\omega_{LH} \approx \omega_{pi}^2/(1+\omega_{pe}^2/\omega_{ce}^2)$ is the lower hybrid frequency and $\omega = 2\pi \times 4.6$ GHz is the launched wave frequency. Experimental results suggest that interactions between LH waves and the scrape off layer (SOL) plasma can have a substantial impact on the operational effectiveness of a LHCD system at high density.

Bremsstrahlung emission in the 50-200 keV range can be taken as a proxy for the population of fast electrons generated by LHCD. Bremsstrahlung on C-Mod is diagnosed with a 32-chord hard x-ray (HXR) camera [10] with simultaneous spatial, temporal, and energy resolving capabilities. Through experiments conducted during the 2008 run campaign, it was discovered that, for single null discharges with line averaged densities in excess of 10^{20} m^{-3}, the fast electron bremsstrahlung emissivity (and thus the population of fast electrons carrying the non-inductive current) was 2–3 orders of magnitude lower than is predicted by a fast electron bremsstrahlung synthetic diagnostic in the ray tracing/Fokker-Planck solver package GENRAY/CQL3D [11, 12, 13]. Figure 1 shows that the experimental HXR data (small symbols) diverges from the $1/\bar{n}_e$ trend predicted by the CQL3D synthetic diagnostic (solid line) for $\bar{n}_e > 10^{20}$ m^{-3}. Current drive efficiency is also predicted to scale as $1/n_e$ based on a simple theoretical model [1, 14]. This limit for production of non-thermal electrons by LHCD is observed at a significantly lower density than was expected based on previous results from other experiments for which wave accessibility (i.e. mode conversion from the slow wave to the fast wave) or parametric decay instabilities set the LHCD density limit. The scaling of the density limit with magnetic field and $n_{||}$ also eliminates these phenomena as possible explanations for the C-Mod results.

Parallel electric currents in the SOL are observed during high power LHCD at high density. The direction of the SOL currents for lower- and upper-single-null configurations is the same as the plasma current inside the last closed flux surface (LCFS). Equal and opposite SOL currents are measured on the inner and outer divertors, with the circuit completed through the vacuum vessel wall. The magnitude of the SOL current increases rapidly across the same range of densities for which the core X-ray emission drops, i.e. $\bar{n}_e > 1 \times 10^{20}$ m^{-3}. The increase in SOL current is well correlated with an increase in ion saturation current, I_{sat}, and thus plasma density, at the ion collecting end of the field line. A modification of density in the SOL of this magnitude indicates strong absorption of the LH waves outside the LCFS.

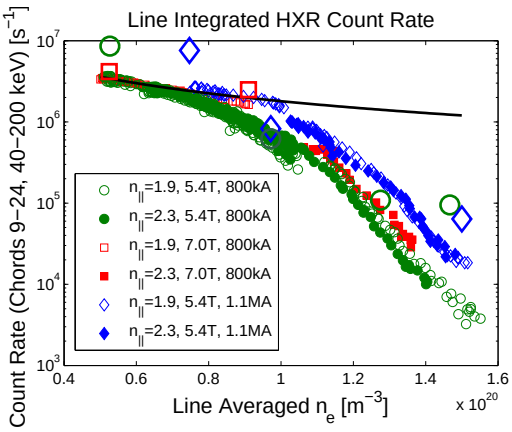

FIG. 1. Comparison of fast electron bremsstrahlung emission predicted by GENRAY/CQL3D code package with a 2-dimensional SOL model in GENRAY including the effects of collisional damping in the SOL. Experimental count rates have been normalized to $P_{LH}^{0.5}$. The large symbols represent simulations while the small symbols are experimental data. The solid line represents a $1/n_e$ trend as predicted by GENRAY/CQL3D without a SOL. All discharges plotted are single null.

The core bremsstrahlung and SOL current observations suggest that power absorption is shifting from inside the LCFS into the SOL as density increases. By including collisional absorption of the LH waves [15] and a SOL in the ray tracing model, agreement between modeling and experimental results is dramatically improved at high density [5, 6, 7]. Figure 1 shows a comparison between the experimental data and the model including absorption in the SOL. The observed density limit on C-Mod appears to be a consequence of poor ray penetration to the hot plasma core and weak single pass absorption inside the LCFS, combined with a loss mechanism in the SOL such as collisional damping.

2. Sensitivity to Plasma Topology

Experiments during the 2010 campaign on C-Mod show that plasma topology plays an important role in the LHCD density limit. Figure 2 shows the line integrated HXR emission for upper single null (USN), lower single null (LSN), double null (DN), and inner wall limited discharges on C-Mod. HXR emission increases by two orders of magnitude at $\bar{n}_e \sim 1.5 \times 10^{20}$ m^{-3} in limited discharges (stars) as compared to single null (circles), and an increase of nearly an order of magnitude in double null (triangles). The HXR emission in limited discharges lies on the $1/\bar{n}_e$ trend line as predicted by GENRAY/CQL3D when run without a SOL. This $1/\bar{n}_e$ trend extends up to a value of 1.6×10^{20} m^{-3}. Above this density the accessibility of the LH waves is expected to be marginal (i.e. the slow and fast wave roots of the dispersion relation may coalesce). HXR emission in DN configuration deviates from the $1/\bar{n}_e$ trend above $\bar{n}_e \sim 1 \times 10^{20}$ m^{-3}, although not as steeply as in lower null. Non-thermal electron cyclotron emission (ECE) trends similarly as a function of $\bar{n}_e$ and configuration.

The double null discharges were fueled both by high field side (HFS) and low field side (LFS) gas puffing, although no clear difference in bremsstrahlung emission is seen between the two gas puffing locations. The single null and limited discharges were fueled on the LFS. The elongation of high density inner wall limited discharges was varied from $\kappa = 1.15$ to $\kappa = 1.5$ to determine if plasma shaping has an effect on the density limit. These experiments showed that HXR emission in limited discharges is not sensitive to changes in plasma elongation.

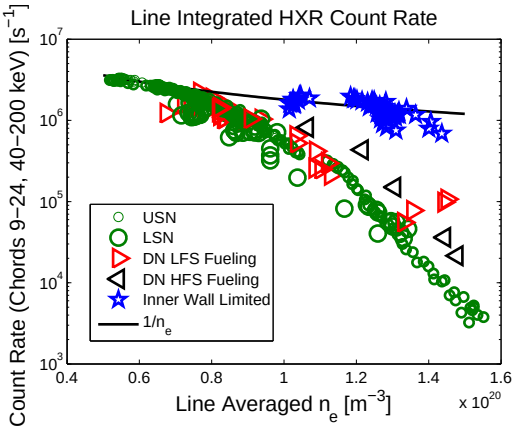

FIG. 2. Comparison of fast electron bremsstrahlung emission as a function of density for different plasma topologies. Double null and particularly limited discharges show a significant increase in fast electron bremsstrahlung over single null discharges. The solid line represents a $1/n_e$ trend. All discharges plotted are at 800 kA and 5.4 T. Diverted discharges have plasma–inner wall gaps greater than 10 mm.

Reciprocating Langmuir probe measurements of the SOL electron density profiles in high density ($\bar{n}_e \sim 1.3 \times 10^{20}$ m^{-3}) discharges show a significant difference between limited and diverted configurations. The SOL n_e profiles for limited and LSN discharges are plotted in Figure 3. There is a small increase in SOL density during LH for the limited case, particularly for $\rho > 15$ mm. The changes in the SOL density profile during LH in LSN are much more dramatic. The density at $\rho = 20$ mm increases by an order of magnitude during LH. The increase in density in the far SOL is so severe that the profile is non-monotonic. The SOL T_e profiles do not change significantly during LH in either configuration. Some of the LH power may be channeled into sustaining the increased density in the far SOL for both the limited and LSN discharges, although the power required to generate the density profile changes in the LSN case would be larger than for the limited case based on the magnitude of the density increase.

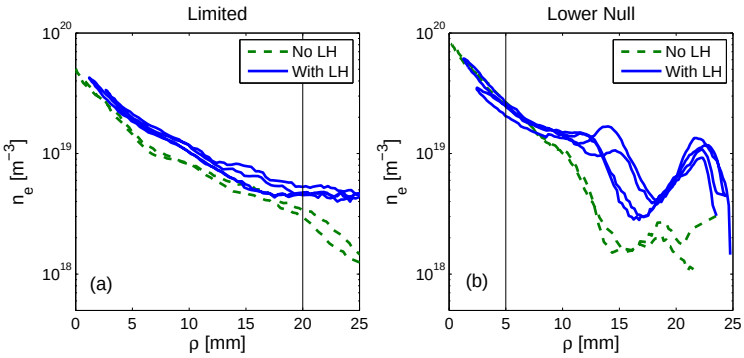

FIG. 3. Electron density profiles in the SOL of high density ($\bar{n}_e \sim 1.3 \times 10^{20}$ m^{-3}) with and without LH for (a) inner-wall limited and (b) LSN discharges. The density profiles are plotted as functions of $\rho = R - R_{LCFS}$ on the midplane. A single in–out sweep before the LH turn on and two in–out sweeps during LH are shown for both configurations. Limited discharges exhibit a noticeable increase in density for $\rho > 15$ mm. The density profile in the far SOL increases more dramatically during LH in LSN discharges. Vertical lines indicate the position of the main plasma limiter for each discharge. Both discharges are at 800 kA, 5.4 T.

3. Sensitivity to Plasma–Inner Wall Gap

The plasma–inner wall gap was systematically scanned in upper null discharges to determine the threshold inner gap for increased HXR emission. Dynamic scans of the inner gap in both directions (inner wall limited to USN and USN to inner wall limited) show that HXR emission is nearly constant for inner gaps greater than ~ 5 mm, and that HXR emission is anti-correlated with inner gap below ~ 5 mm. Figure 4 shows the time evolution of two discharges with dynamic inner gap scans. Although the line averaged density varies slightly during LHCD, non-thermal emission is clearly higher for plasma–inner wall gaps of less than ~ 5 mm.

Figure 5 shows HXR emission as a function of density for plasma–inner wall gaps of 10–15 mm, 3–5 mm, and 0 mm (i.e. inner wall limited). Some of the increase in HXR emission at zero plasma–inner wall gap can be explained by an increase in Z_{eff} in limited discharges or by thick-target bremsstrahlung from fast electrons striking the inner wall. The non-thermal ECE, which is not sensitive to Z_{eff} or thick target bremsstrahlung, also shows an increase in the population of non-thermal LH generated electrons as the plasma–inner wall gap decreases (see Figure 6).

High density single null discharges with small inner gaps do exhibit signs of current drive despite weaker non-thermal emission as compared to inner wall limited discharges. The relative change in loop voltage, $\Delta V/V$, for a limited discharge was 0.17, while the relative change in loop voltage was 0.12 for an USN discharge with an inner gap of 4 mm. Non-thermal ECE and HXR emission is approximately double in the limited discharge as compared to the small gap discharge. The two discharges have the same net LH power (650 kW), plasma current (800 kA), toroidal field (5.4 T), and line averaged density ($\bar{n}_e = 1.3 \times 10^{20}$ m^{-3}).

4. Sensitivity to Plasma Temperature

The results discussed in the preceding sections were obtained in the low single-pass absorption regime. It was hoped that by increasing the plasma temperature, and thus the damping of the rays on the first pass through the plasma, that the effect of parasitic edge

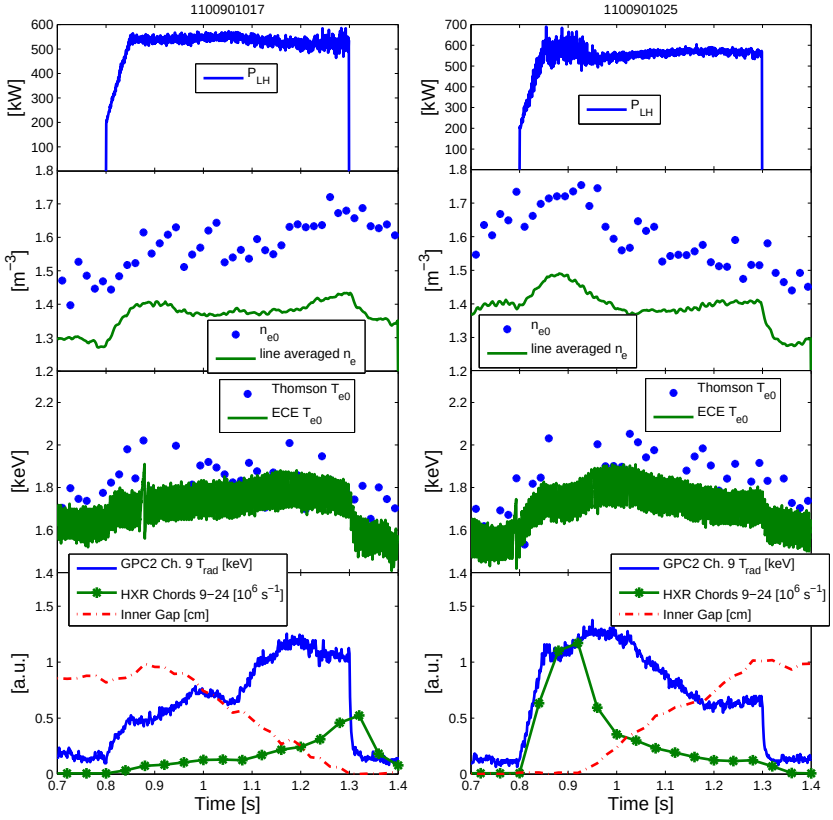

FIG. 4. Plasma evolution during plasma–inner wall gap scans in single null. ECE and HXR emission are anti-correlated with inner gap for gaps below ∼ 5 mm. HXR emission is not sensitive to inner gaps greater than ∼ 5 mm. GPC2 Channel 9 (bottom panels) primarily measures non-thermal emission. Both discharges are at 800 kA, 5.4 T.

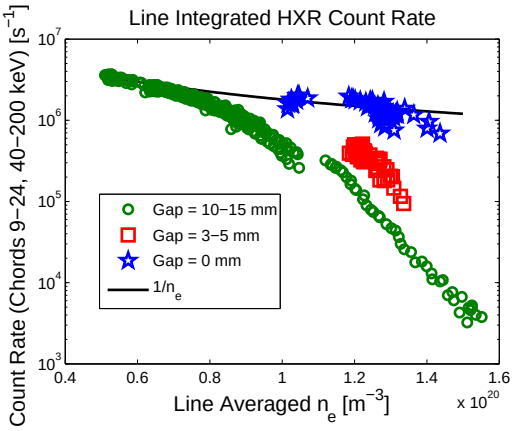

FIG. 5. Comparison of fast electron bremsstrahlung emission as a function of density for different plasma–inner wall gaps. The solid line represents a $1/n_e$ trend. All discharges plotted are 800 kA, 5.4 T.

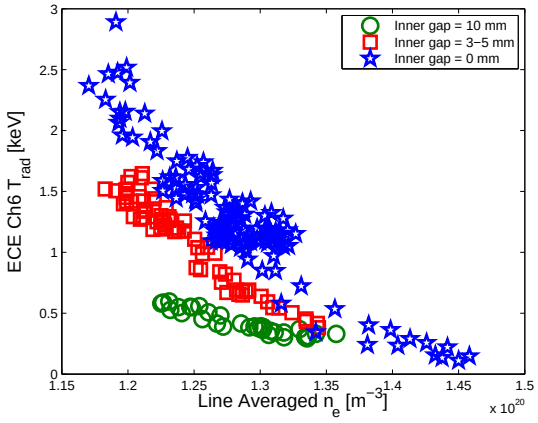

FIG. 6. Comparison of non-thermal ECE as a function of density for different plasma–inner wall gaps. The frequency of ECE channel 6 maps to a major radius outside the LCFS. All discharges plotted are at 800 kA and 5.4 T.

losses would be reduced. The central electron temperatures of L-mode plasma targets ($\bar{n}_e = 1.2 - 1.45 \times 10^{20}$ m^{-3}, $I_p = 1.1$ MA, $B_t = 5.4$ T) were raised by applying 1.0, 2.0, and 2.5 MW of ion cyclotron range of frequency (ICRF) minority heating at 78 and 80 MHz. The temperature profiles in the discharges with ICRF were highly peaked and $T_{r/a=0.9}$ was in the range of 200–400 eV. These discharges exhibited an increase in T_{e0} from 2 keV for the ohmic targets to over 4 keV with 2.5 MW of ICRF. The HXR count rates show little increase with ICRF heating in L-mode, although it should be noted that high power ICRF causes a large increase in the background HXR level. This increase in background makes direct comparison of ohmic and ICRF heated discharges difficult. Non-thermal ECE, which is not adversely effected by ICRF heating, is used for comparison instead. Figure 7 shows the non-thermal ECE as a function of density for L-mode discharges with varying ICRF power levels. A small increase in non-thermal emission is seen with increased ICRF power. Non-thermal emission in limited discharges is significantly higher than for ICRF heated, diverted discharges.

Results from the FTU LHCD experiment suggest that the LHCD density limit can be overcome by raising the temperature in the plasma edge ($r/a > 0.8$) [16, 17]. The I-mode confinement regime on C-Mod consists of an H-mode like temperature pedestal at the plasma edge with an L-mode like density profile [18, 19]. Comparing I-mode and L-mode discharges with similar density profiles and core temperatures provides a convenient way to assess the effect of edge temperature on the LHCD density limit. LHCD was applied to I-mode discharges ($I_p = 900$ kA, $P_{ICRF} = 2.8 - 3.8$ MW) with $T_{e0} \sim 5$ keV and $T_{r/a=0.9} = 500-800$ eV. The non-thermal ECE signatures increase by a factor of ~ 2 in I-mode as compared to L-modes with similar core temperatures (see Figure 8). This mod-

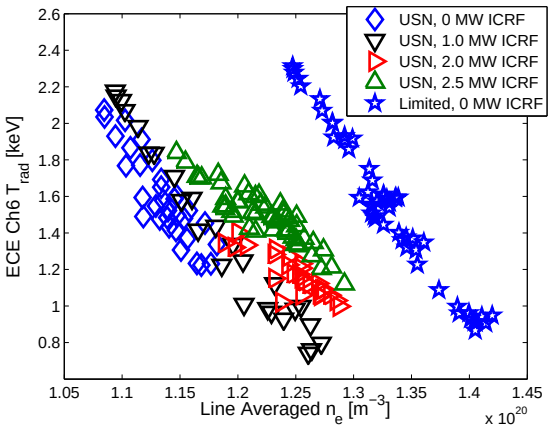

FIG. 7. Comparison of non-thermal electron cyclotron emission as a function of density for different ICRF power levels. The solid line represents a $1/n_e$ trend. All discharges plotted are 1.1 MA, 5.4 T.

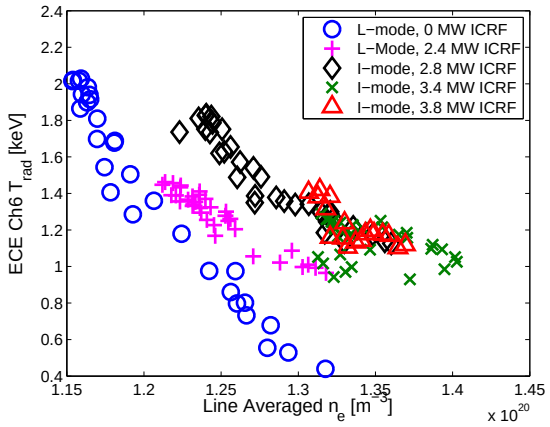

FIG. 8. Comparison of non-thermal ECE as a function of density for L- and I-mode discharges at varying ICRF power levels. The frequency of ECE channel 6 maps to a major radius outside the LCFS. All discharges plotted are 900 kA, 5.6 T.

est increase in non-thermal emission as edge temperature increases is smaller compared to the effect of changing between diverted and limited configurations. Thus, increasing edge T_e does not appear to eliminate the density limit for LHCD in a diverted tokamak.

5. Discussion and Conclusions

Simulations of parasitic collisional absorption in the SOL show that much of the absorption occurs in the region between the lower divertor and the mid-plane on the HFS [20]. The density at the inner wall is typically above the slow wave cutoff ($n_e = 2.6 \times 10^{17}$ m^{-3} at 4.6 GHz) even for large plasma–inner wall gaps (> 10 mm). The LH waves are able to propagate between the LCFS and the inner wall and parasitic collisional absorption may occur in this region. Operating in a regime with little (small plasma–inner wall gap) or no (inner wall limited) space for the waves to propagate between the last closed flux surface and the conducting wall on the HFS may reduce or eliminate the parasitic losses in the SOL. Changes in the SOL behavior and neutral pressure as a result of the variation in plasma shape and position likely play an important role as well.

Although the strongest non-thermal electron signatures are observed in the limited configuration, limited discharges are of less interest to the C-Mod advanced scenarios program due to the difficulty in accessing high confinement regimes (H- and I-mode) without a diverted plasma. The increase in non-thermal emission in double null discharges, and also in single null discharges with small (< 5 mm) plasma–inner wall gaps, is encouraging and may be enhanced by operating in double null with a similarly small inner gap. This synergistic effect may also exist in conjunction with additional ICRF heating. Launching LH waves from the HFS wall of the tokamak may also increase the effectiveness of LHCD at high density, although constructing a LH launcher for the HFS presents considerable technical difficulties. Additional experimental and modeling work is necessary to identify the optimal conditions for LHCD at high density in a diverted configuration.

These results show a clear difference in the phenomenology of the LHCD density limit between diverted and limited configurations. Much of the prior investigation of LHCD at high densities was conducted in circular, limited tokamaks such as Alcator C [21] and FTU [22, 16, 17]. Although the experiments on C-Mod show no dependence on elongation, the difference between limited and diverted plasmas is significant and this may explain

the unexpectedly low density limit encountered for diverted discharges in C-Mod. Future LHCD experiments in diverted, high-density discharges, such as those anticipated for ITER [23, 24], need to be considered in the context of the density limit for diverted tokamaks.

Acknowledgments

The authors would like to thank the C-Mod LHCD engineering team for their efforts. This work supported by USDOE awards DE-FC02-99ER54512 and DE-AC02-76CH03073.

References

[1] FISCH, N. J. et al., Physical Review Letters **45** (1980) 720.
[2] BONOLI, P. T. et al., Fusion Science and Technology **51** (2007) 401.
[3] HUTCHINSON, I. H. et al., Physics of Plasmas **1** (1994) 1511.
[4] WILSON, J. et al., Nuclear Fusion **49** (2009) 115015.
[5] WALLACE, G. M. et al., Bull. Am. Phys. Soc. **53** (2008) 222.
[6] WALLACE, G. M. et al., Observations of lower hybrid wave absorption in the scrape off layer of a diverted tokamak, in *RADIO FREQUENCY POWER IN PLASMAS: Proceedings of the 18th Topical Conference*, edited by BOBKOV, V. et al., volume 1187, pages 395–398, American Institute of Physics, Melville, NY, 2009.
[7] WALLACE, G. M. et al., Physics of Plasmas **17** (2010) 082508.
[8] HOOKE, W., Plasma Physics and Controlled Fusion **26** (1984) 133.
[9] TAKASE, Y. et al., Physics of Fluids **28** (1985) 983.
[10] LIPTAC, J. et al., Review of Scientific Instruments **77** (2006) 103504.
[11] SMIRNOV, A. P. et al., Bull. Am. Phys. Soc. **40** (1995) 1837.
[12] HARVEY, R. W. et al., The CQL3D Fokker-Planck Code, in *Proceedings of the IAEA Technical Committee Meeting on Simulation and Modeling of Thermonuclear Plasmas*, pages 489–526, 1992.
[13] HARVEY, R. et al., The CQL3D Fokker-Planck Code, Technical report, General Atomics, 1992.
[14] Fisch, N. J., Reviews of Modern Physics **59** (1987) 175.
[15] BONOLI, P. T. et al., Physics of Fluids **29** (1986) 2937.
[16] CESARIO, R. et al., Lower hybrid current drive at ITER-relevant high plasma densities, in *RADIO FREQUENCY POWER IN PLASMAS: Proceedings of the 18th Topical Conference*, edited by BOBKOV, V. et al., volume 1187, pages 419–422, American Institute of Physics, Melville, NY, 2009.
[17] CESARIO, R. et al., Nat. Commun. **1** (2010) 55.
[18] WHYTE, D. et al., Nuclear Fusion **50** (2010) 105005.
[19] MCDERMOTT, R. M. et al., Physics of Plasmas **16** (2009) 056103.
[20] WILSON, J. R. et al., Bull. Am. Phys. Soc. (2009) 8007P.
[21] PORKOLAB, M. et al., Physical Review Letters **53** (1984) 450.
[22] PERICOLI-RIDOLFINI, V. et al., Physical Review Letters **82** (1999) 93.
[23] AYMAR, R. et al., Plasma Physics and Controlled Fusion **44** (2002) 519.
[24] HOANG, G. et al., Nuclear Fusion **49** (2009) 075001.